Biochemical Journal (2021) **478** 533–551
https://doi.org/10.1042/BCJ20200627

Research Article

Temporal modulation of the NF-κB RelA network in response to different types of DNA damage

Amy E. Campbell[1,*], Catarina Ferraz Franco[1,*], Ling-I Su[2], Emma K. Corbin[2], Simon Perkins[3], Anton Kalyuzhnyy[3], Andrew R. Jones[3], Philip J. Brownridge[1], Neil D. Perkins[2] and Claire E. Eyers[1]

[1]Centre for Proteome Research, Department of Biochemistry and Systems Biology, Institute of Systems, Molecular and Integrative Biology, University of Liverpool, Liverpool L69 7ZB, U.K.; [2]Faculty of Medical Sciences, Biosciences Institute, Newcastle University, Newcastle Upon Tyne NE2 4HH, U.K.; [3]Department of Biochemistry and Systems Biology, Institute of Systems, Molecular and Integrative Biology, University of Liverpool, Liverpool L69 7ZB, U.K.

Correspondence: Claire E. Eyers (ceyers@liverpool.ac.uk)

Different types of DNA damage can initiate phosphorylation-mediated signalling cascades that result in stimulus specific pro- or anti-apoptotic cellular responses. Amongst its many roles, the NF-κB transcription factor RelA is central to these DNA damage response pathways. However, we still lack understanding of the co-ordinated signalling mechanisms that permit different DNA damaging agents to induce distinct cellular outcomes through RelA. Here, we use label-free quantitative phosphoproteomics to examine the temporal effects of exposure of U2OS cells to either etoposide (ETO) or hydroxyurea (HU) by monitoring the phosphorylation status of RelA and its protein binding partners. Although few stimulus-specific differences were identified in the constituents of phosphorylated RelA interactome after exposure to these DNA damaging agents, we observed subtle, but significant, changes in their phosphorylation states, as a function of both type and duration of treatment. The DNA double strand break (DSB)-inducing ETO invoked more rapid, sustained responses than HU, with regulated targets primarily involved in transcription, cell division and canonical DSB repair. Kinase substrate prediction of ETO-regulated phosphosites suggest abrogation of CDK and ERK1 signalling, in addition to the known induction of ATM/ATR. In contrast, HU-induced replicative stress mediated temporally dynamic regulation, with phosphorylated RelA binding partners having roles in rRNA/mRNA processing and translational initiation, many of which contained a 14-3-3ε binding motif, and were putative substrates of the dual specificity kinase CLK1. Our data thus point to differential regulation of key cellular processes and the involvement of distinct signalling pathways in modulating DNA damage-specific functions of RelA.

Introduction

RelA, also known as p65, is a key member of the NF-κB family of transcription factors, which serve as 'master regulators' of the cellular inflammatory and stress responses, and are key components that maintain tissue homeostasis and contribute to aging. As part of a functional homo- or hetero-dimer (preferentially with p50), RelA regulates a diverse set of genes involved in core cellular processes such as inflammation, proliferation, apoptosis and metastasis [1]. The precise functional roles (the complement of genes transcribed) of RelA are governed both by its post-translational modification (PTM) status, and the transcriptional complexes formed, which are themselves regulated in a co-ordinated fashion through numerous cell signalling pathways [2–4]. PTMs have the potential to regulate many aspects of NF-κB signalling in response to different stimuli, including nuclear translocation, protein-protein or protein-DNA interactions, and stability, often working in a combinatorial fashion to regulate complex formation and transcriptional output.

*These authors contributed equally to this work.

Received: 12 August 2020
Revised: 11 January 2021
Accepted: 12 January 2021

Accepted Manuscript online: 13 January 2021
Version of Record published: 10 February 2021

Biochemical Journal (2021) 478 533–551
https://doi.org/10.1042/BCJ20200627

While NF-κB signalling is commonly associated with inflammation and the immune response, these pathways also play key roles in the cellular response to DNA stress. Consequently, aberrant NF-κB signalling is observed in, and often a contributing factor to, many human diseases, including autoimmune disorders, chronic inflammatory diseases, and cancer [1,5–7]. NF-κB signalling is also central to age-related degenerative diseases as a result of accumulated age-related DNA damage [8]. The pro-survival effects mediated by NF-κB in response to specific-types of DNA damage in part explains the cellular resistance to chemotherapy. Hence, a clear understanding of NF-κB signalling in response to DNA damage is important, not only in the context of ageing, but also to enhance cancer treatment strategies.

In response to different types of DNA damage, cells invoke specific responses that promote DNA repair, induce cell cycle arrest, regulate cell death or induce cellular senescence [9,10]. For example, inhibition of DNA replication using hydroxyurea (HU), which inhibits ribonuclease diphosphate reductase, arrests cells primarily in S-phase [11–15]. In contrast, agents such as etoposide (ETO), which induces DNA double stranded breaks (DSBs) by preventing topoisomerase II-mediated DNA re-ligation during replication and cell division, cause cells to accumulate in the G2/M phase of the cell cycle [16–19]. Whilst activation of NF-κB-responsive genes following DNA stress has been investigated, the mechanisms of regulating these differential outputs remain poorly characterised [1,5–7]. Both HU and ETO invoke a DNA damage stress response through ataxia telangiectasia mutated (ATM)-mediated activation of NF-κB, leading to elevated levels of NF-κB targets such as Survivin and Bcl-xL. However, these two types of DNA damaging agents result in distinct cellular responses in a variety of tumour-derived cell lines and in primary cells cancer cells, in part due to induction of different NF-κB gene expression patterns [19–22]; HU mediates a pro-apoptotic response, while an anti-apoptotic response results following cellular exposure to ETO [22]. Differential involvement of p53 in regulating NF-κB outputs in response to these different types of DNA damaging agents also plays a role: while the transcriptional response to HU requires p53 for both early and late NF-κB target gene expression, NF-κB-mediated transcription in response to ETO is independent of p53 [22].

The activity of all NF-κB subunits, including RelA, is extensively controlled by a variety of PTMs including phosphorylation, acetylation, methylation, glycosylation, proline isomerisation, cysteine oxidation and ubiquitination [23–26]. Of these, phosphorylation accounts for the majority of the well-understood dynamic mechanisms of regulation, both direct e.g. pSer45 modulation of DNA binding [26], and indirect e.g. pSer276, which controls a number of other PTMs, including ubquitination and thus RelA stability [2,27,28]. Of relevance here, Thr505 phosphorylation has been shown to mediate pro-apoptotic effects upon cisplatin-induced DNA damage [29,30]. Given the complexity of NF-κB signalling, unravelling the mechanisms by which NF-κB subunits, particularly RelA, induce differential transcriptional specificity in a context-dependent manner is challenging.

The sensitivity and versatility of mass spectrometry (MS) makes it ideal for the study (identification and quantification) of dynamic PTMs and the regulated binding partners of transcription factors and their transcriptional complexes. Here we utilise a label free phosphoproteomics approach to map DNA damage-induced changes in RelA binding partners and their phosphorylation status, in response to either HU-induced replicative stress, or ETO-mediated DSB. We find that whilst RelA associated proteins remain largely unchanged as a function of DNA stress, there are notable changes in the dynamics of phosphorylation of the RelA-interactome as a function of treatment. These findings point towards different signalling pathways directing the formation of specific RelA networks dependent on the type of DNA damage that likely help direct transcriptional output and thus the cellular response.

Materials and methods

Reagents and antibodies

Unless otherwise stated, general lab reagents were purchased from Sigma Aldrich and were of the highest quality available. The following primary antibodies were used for immunoblotting at 1/1000 dilution in 5% (w/w) BSA overnight at 4°C: anti-RelA (sc-372, Santa Cruz), anti-HA (Merck, HA-7), anti phospho-histone H2AX (#2577, Cell Signalling), anti-PAK4 (#3242, Cell Signaling Technologies), anti-Karyopherin-β1 H-7 (sc-137016, Santa Cruz). Secondary anti-rabbit IgG (7074S, Cell Signalling Technology) was used at 1/5000 dilution following membrane incubation with VeriBlot (1/400 dilution, ab131366 Abcam).

Generation and culture of HA-RelA U2OS cells

The HA-RelA U2OS cell line was generated by transfecting wild-type U2OS cells with the plasmid pRcRSV HA RelA plasmid, which also expresses the neomycin gene. Cells stably expressing HA tagged RelA were then

selected by treatment with G418 (600 μg/ml, Melford Chemicals, cat. no. G0175), with pooled populations of cells used in experiments.

Cell treatment and lysis

U2OS cells expressing HA-RelA (or HA control cells) were cultured in DMEM supplemented with 10% (v/v) fetal bovine serum, penicillin (100 U/ml), streptomycin (100 U/ml), and L-glutamine (2 mM) at 37°C, 5% CO_2. Once 80% confluence was reached, cells were treated with either 50 μM etoposide (50 mM stock solution in DMSO) or 2 mM hydroxyurea (100 mM stock solution in DMEM, 5% DMSO), by addition to the culture media, for the indicated times. Control cells were grown for the maximum time (2 h) in 0.1% (v/v) DMSO. After removal of the media, cells were washed three times with ice cold PBS. For proteomics analysis, cells were harvested in 400 μl of lysis buffer (100 mM Tris–HCl pH 8.0, 150 mM NaCl, 0.5 mM EDTA, 0.5% (v/v) Triton X-100, 0.5% (v/v) NP-40, 1× PhosSTOP™ phosphatase inhibitor cocktail tablet (Roche), 1× cOmplete™ Protease Inhibitor Cocktail (Roche), 50 U/ml of benzonase) into 1.5 ml microtubes using a cell scraper. Cells were then incubated on ice for 120 min to permit cell lysis to occur. Cell lysates were then cleared by centrifugation (16 000×***g***, 10 min, 4°C) and protein concentration was determined using the Bradford assay. A total protein amount of 4 mg was set aside for HA-RelA immunoprecipitation. Cell treatment and lysis was performed in triplicate to obtain three independent biological replicates for each treatment condition and control (untreated) cells for proteomics analysis.

For the RelA co-immunoprecipitation studies, HA-RelA or HA control U2OS cells were lysed in IP lysis buffer (25 mM Tris pH 8, 0.15 M NaCl, 0.1% (w/v) NP-40, 1 mM EDTA, 1 mM DTT, containing 1× PhosSTOP™ phosphatase inhibitor cocktail tablet (Roche), and cOmplete™ Protease Inhibitor Cocktail (Roche)) after treatment with either ETO or HU as above. Protein concentration was determined using a BCA protein assay kit according to the manufacturer's instructions (Thermo Scientific).

Immunoprecipitation of HA-RelA for proteomics

Pierce™ Anti-HA Magnetic Beads were washed with 0.05% (v/v) TBST and then with lysis buffer prior to addition of 4 mg cleared cell lysate (at a ratio of beads to protein of 1:2000). Beads and lysate were incubated overnight using an end-over-end rotor at 4°C. Beads were then collected using a magnetic stand and washed three times with wash buffer (40 mM Tris-HCl pH 8.0, 0.1% (v/v) NP-40, 1 mM EGTA, 6 mM EDTA, 6 mM DTT, 0.5 M NaCl, 1× PhosSTOP™ phosphatase inhibitor cocktail tablet (Roche), 1× cOmplete™ Protease Inhibitor Cocktail (Roche)); one time with HPLC grade water and finally, three times with 25 mM ammonium bicarbonate (AMBIC). To recover the immunoprecipitated material, the beads were resuspended in 100 μl of 25 mM AMBIC to which 6 μl of a 1% (w/v) solution of RapiGest (Waters, UK) in 25 mM AMBIC was added. Samples were then heated to 80°C for 10 min. Supernatants containing the eluted proteins were recovered using a magnetic stand and used for in-solution digestion.

Co-immunoprecipitation of HA-RelA and immunoblotting

Pierce™ protein A/G Magnetic Beads were incubated with anti-HA antibody (sc-7392, Santa Cruz Biotechnology) in 5% (w/w) BSA for 3 h at 4°C, using 10 μl beads and 1 μg antibody per IP. Beads were washed three times with IP lysis buffer (500 μl) and incubated overnight using an end-over-end rotor at 4°C. Beads were then collected using a magnetic stand and washed three times with wash buffer prior to elution of bound protein in 30 μl of 2× SDS loading buffer for SDS–PAGE and immunoblotting.

In-solution digestion and TiO_2-based enrichment of phosphorylated peptides

Samples were digested with trypsin and subjected to TiO_2-based phosphopeptide enrichment as previously described [31]. In brief, disulfide bonds were reduced by addition of DTT to a final concentration of 4 mM (10 min, 60°C with gentle agitation). Samples were cooled to room temperature and free cysteines alkylated with 14 mM iodoacetamide (30 min, RT), prior to addition of DTT (to 7 mM final) to quench excess iodoacetamide. Samples were digested with trypsin (1:50 trypsin:protein ratio) overnight at 37°C with light agitation (450 rpm on an Eppendorf thermomixer). Digestion was stopped by the addition of trifluoracetic acid (TFA) to a final concentration of 0.5% (v/v) and incubated for 45 min at 37°C. RapiGest insoluble hydrolysis products were removed by centrifugation (13 000×***g***, 15 min, 4°C). Digested samples were dried by vacuum centrifugation and resolubilized in TiO_2 loading buffer (80% acetonitrile, 5% TFA, 1 M glycolic acid) to achieve a peptide concentration of 1 μg/μl and sonicated for 10 min. TiO_2 beads (50 μg/μl in loading buffer) were mixed at

Biochemical Journal (2021) 478 533–551
https://doi.org/10.1042/BCJ20200627

1400 rpm (with intermittent vortexing to prevent the beads from pelleting) with the resuspended peptides (bead:protein ratio of 5:1) for 20 min at RT. TiO_2 beads were recovered by centrifugation (2000× ***g***, 1 min) and washed successively for 10 min (1400 rpm) with 150 μl of loading buffer, 80% acetonitrile 1% TFA, then 10% acetonitrile, 0.2% TFA. Prior to elution, beads with bound phosphopeptides were dried to completion by vacuum centrifugation. Bound phosphopeptides were then eluted by addition of 100 μl of 1% (v/v) ammonium hydroxide and then with 100 μl of 5% (v/v) ammonium hydroxide. Both elutions were combined and dried by vacuum centrifugation.

Liquid chromatography-tandem mass spectrometry (LC-MS/MS) analysis

Phosphopeptide enriched samples were analysed by LC-MS/MS using an Ultimate 3000 RSLC™ nano system (Thermo Scientific, Hemel Hempstead) coupled to a QExactive HF mass spectrometer (Thermo Scientific). The samples were loaded onto a trapping column (Thermo Scientific, PepMap100, C18, 300 μm × 5 mm), using partial loop injection, for seven minutes at a flow rate of 4 μl/min with 0.1% (v/v) FA, and resolved on an analytical column (Easy-Spray C18 75 μm × 500 mm 2 μm column) using a gradient of 97% A (0.1% formic acid), 3% B (99.9% ACN 0.1% formic acid) to 60% A, 40% B over 80 min at a flow rate of 300 nL/min. Data-dependent acquisition employed a 60 000 resolution full-scan MS scan (MS1) with AGC set to 3×10^6 ions with a maximum fill time of 100 ms. The 10 most abundant peaks were selected for MS/MS using a 60 000 resolution scan (AGC set to 1×10^5 ions with a maximum fill time of 100 ms) with an ion selection window of 1.2 m/z and a normalised collision energy of 29. A 20 sec dynamic exclusion window was used to minimise repeated selection of peptides for MS/MS.

LC-MS/MS data analysis

LC-MS/MS files were aligned in Progenesis QI for Proteomics label-free analysis software. At this stage, no normalisation was performed and an aggregate file containing raw abundances from all the peaks across all runs was exported from Progenesis. These files were searched against UniProt Human reviewed protein database (downloaded December 2015; 20 187sequences) using MASCOT (v 2.6) within Proteome Discoverer (v. 1.4; Thermo Scientific). Parameters were set as follows: MS1 tolerance of 10 ppm, MS2 mass tolerance of 0.01 Da; enzyme specificity was defined as trypsin with two missed cleavages allowed; Carbamidomethyl Cys was set as a fixed modification; Met oxidation, and Ser/Thr/Tyr/His phosphorylation were defined as variable modifications. Data were filtered to a 1% false discovery rate (FDR) on peptide spectrum matches (PSMs) using automatic decoy searching with MASCOT. *ptm*RS node with Proteome Discoverer was used to determine phosphosite localization confidence. To match *ptm*RS scores to Progenesis MASCOT output files, two rounds of Excel vlookup functions were used: (1) to retrieve scan numbers from the TOP hit per feature number, and (2) to retrieve *ptm*RS score using the corresponding scan number.

'Normalyzer' software [32] was used to assess the suitability of various types of normalization strategies on the data. Amongst normalization strategies, VSN-G (group-based variance stabilizing normalisation) performed well under various quality control metrics indicating a reduction in technical variance. The 'vsn' R/Bioconductor package [33] was then used to normalize log transformed peptide abundance data for the subsequent stages of analysis. Pairwise *t*-test and cross condition ANOVA statistical testing, followed by Benjamini–Hochberg global correction was subsequently also performed in R for any replicate groups without missing values. Unless otherwise described, all plots were generated in R.

Network analysis

All proteins with quantified phosphopeptides in two or more (of the three) repeats of any condition were combined for network analysis of RelA-associated proteins. Common contaminants that bind non-specifically in IP experiments were removed by filtering protein accessions against a CRAPome database (https://www.crapome.org) [34] of contaminants observed with Streptactin-HA IPs from U2OS cells (CC405, CC406 and CC410). All proteins not present in the contaminant database were entered into STRING (https://string-db.org, v11.0) to generate a network of protein associations [35]. The generated network was filtered to contain only high confidence associations (interaction score ≥0.7) with experimental or database evidence only. Proteins with no high confidence interactions were removed from the network and the remaining nodes were clustered using the Kmeans algorithm (K = 9). The resulting network was imported into Cytoscape [36] with nodes recoloured, grouped into the top 9 Kmeans clusters and node shapes for proteins unique to HU or ETO changed to squares or diamonds respectively. For the top 9 Kmeans clusters, nodes corresponding to proteins with

differentially regulated phosphopeptides in response to either HU, ETO or both treatments, with respect to the untreated control, were outlined in red, blue or black respectively.

Functional enrichment analysis

All functional enrichment analysis was performed using the functional annotation tool in DAVID (https://david.ncifcrf.gov, v6.8) against a background of the human proteome [37,38]. For biological process GO term pie charts, all significantly enriched (Benjamini adj.*P*-value ≤ 0.05) GO biological process terms, with associated Benjamini adj.*P*-values, were summarised using REVIGO [39] then visualised with the CirGO Python package [40]. Bubble plots including significantly enriched (Benjamini adj.*P*-value ≤ 0.05) GO biological process (BP), molecular function (MF), cellular component (CC) and overrepresented keywords, filtered to remove duplicate terms, were plotted in R.

Kinase prediction/sequence motif analysis

Kinase-substrate prediction for all differentially regulated (*t*-test, $p \leq 0.05$) phosphosites was performed using NetPhorest [41,42]. Briefly, for all 'class I' phosphorylation sites (*ptm*RS ≥ 0.75) protein identifiers together with the position of the phosphorylated residue were submitted to NetPhorest using the high-throughput web interface, with the top scoring prediction for each site reported. Kinase predictions were summarised for all up- or down-regulated phosphosites with the resulting data plotted in R. For sequence motif analysis, sequence windows encompassing 7 amino acids either side of the phosphorylated residue were extracted for all phosphosites significantly up- or down- regulated (*t*-test, $P \leq 0.05$) with respect to the untreated control. Consensus sequence motifs were generated with iceLogo v1.2 [43] against a background of the precompiled human Swiss-Prot composition using percent difference as the scoring system and a *P*-value cut-off of 0.05. The most confident phosphosite per phosphopeptide was also cross-referenced against data from PeptideAtlas (PA) [64] (2020 build), and from PhosphoSitePlus (PSP) [65] (11/03/20 build), categorising phosphorylation site confidence based on the number of observations - 'High': ≥5 previous observations, very likely true site; 'Medium': 2–4 previous observations, likely true site; 'Low': 1 previous observation, little support that it is a true site; PA only – 'Not phosphorylated': frequently (>5) observed to be not phosphorylated, never observed as phosphorylated; 'Other' – no confident evidence in any category. Observations in PA were counted with a threshold of >0.95 PTM Prophet probability for positive evidence, and ≤0.19 for evidence of not being phosphorylated.

Results

Selection of DNA damage timepoints

To identify changes in the phosphorylation status of RelA and its protein binding partners in response to different types of DNA damage, we first examined the kinetics of DNA damage after treatment with either the DSB inducer ETO, or the replicative stress inducer HU in the HA-RelA U2OS cell line. Using gamma-H2AX as a marker [44,45], we observed rapid DNA damage (within 30 min) following treatment with either ETO or HU (Figure 1; Supplementary Fig. S1). Gamma-H2AX levels peaked faster with ETO than HU, but sustained (and maximal) levels were observed with both agents following ∼2 h of continuous treatment. A time-course of the effect of these different DNA damaging agents on the RelA phosphorylation interactome was therefore evaluated by treatment of the HA-RelA U2OS cells with either ETO or HU for 0, 30, 60 or 120 min prior to immunoprecipitation (IP) of the HA-tagged RelA. Immunoprecipitated proteins were subject to titanium dioxide (TiO_2)-based phosphopeptide enrichment prior to LC-MS/MS with label-free peptide quantification (Figure 1).

Network of RelA-associated proteins

Using the identified (phospho)peptides as proxy for protein identifications, the list of RelA bound proteins under all conditions was filtered against a 'CRAPome' database of contaminants commonly observed in Streptactin-HA IPs from U2OS cells (CC405, CC406 and CC410), which provided the closest match to the experimental workflow described here. Phosphopeptide quantification data was normalised and subjected to ANOVA testing across all conditions, and individual t-tests across all pairs of conditions. Using this list, the temporal effect of treatment with either ETO or HU on RelA bound phosphoproteins was evaluated for all those proteins quantified in at least 2 biological replicates, under a given condition.

To generate a network of high confidence interactors, the remaining 815 RelA-associated proteins combined across all conditions (Supplementary Table S1) were inputted into STRING (v11.0) [35] using experimental

Biochemical Journal (2021) 478 533–551
https://doi.org/10.1042/BCJ20200627

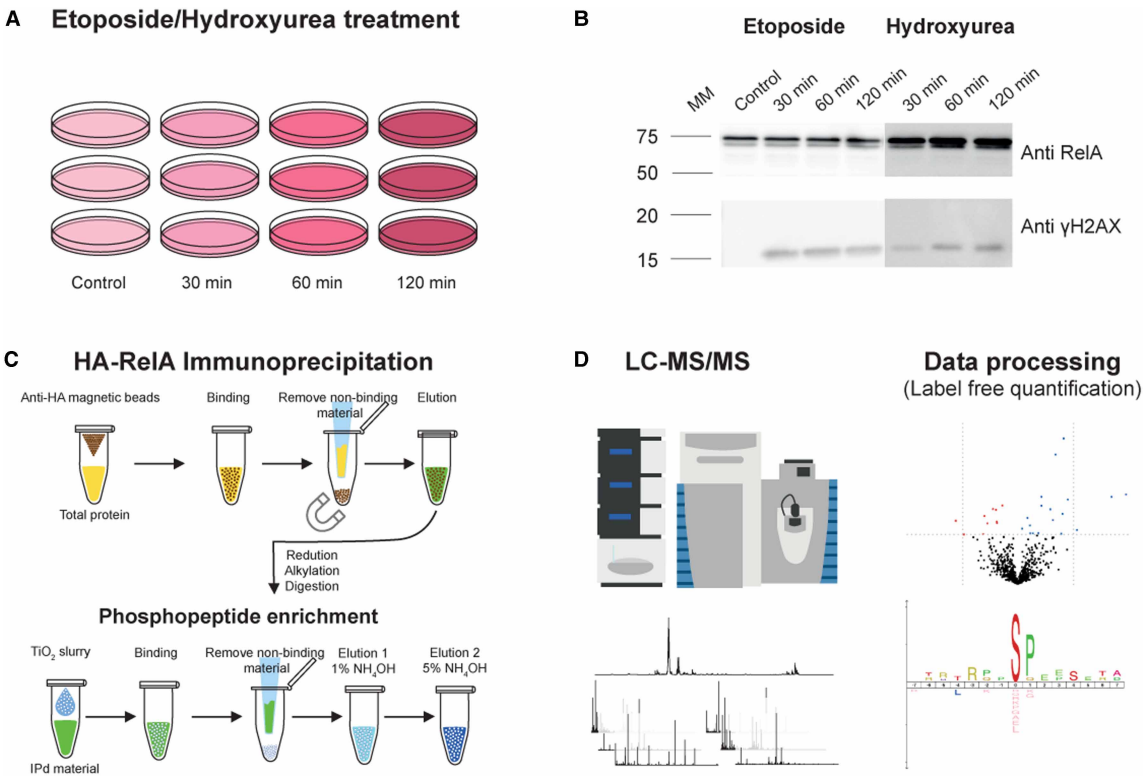

Figure 1. Workflow for evaluation of DNA damage response of HA-RelA U2OS cells with either Etoposide (ETO) or Hydroxyurea (HU).

(A) HA-RelA U2OS cells were treated with either 0.1% DMSO (control), ETO (50 μM) or HU (2 mM) for the times indicated to induce DNA damage. (B) Following treatment with either ETO or HU, HA-RelA U2OS cell lysates were immunoblotted with antibodies against either γH2AX as a marker of DNA damage, or RelA/p65. (C) Workflow for evaluation of the phosphorylated RelA interactome. Cells were treated as in (A), and RelA-bound proteins immunoprecipitated with an anti-HA antibody. Proteins were subjected to tryptic digestion and TiO_2-based phosphopeptide enrichment. (D) Peptides were analysed by LC-MS/MS using a QExactive HF and subjected to label-free quantification following appropriate normalisation.

and database sources only, and clustered using the *K*means algorithm ($k = 9$). Twelve of these proteins failed to yield high confidence interactions and therefore were filtered out of subsequent datasets (Figure 2). Gene Ontology (GO) enrichment analysis of biological function for these 803 proteins within the top 9 network clusters confirmed association of RelA with a number of IκB kinase/NF-κB signalling proteins (Figure 2A), including RelB, c-Rel, p105/p50, p100/p52, IκBα, IκBβ, and the DNA damage response (Figure 2B). Clusters of proteins across a number of core cellular processes were also identified in the RelA interactome, including key proteins involved in cell division, transcriptional regulation, mRNA/rRNA processing and MAPK/ERK/VEGF signalling (Figure 2A–H). Amongst these interactions partners, we also confirmed observation of a number of known RelA binding proteins, including e.g. replication factor C (RFC1), p300, SP1 and HDAC6 [46–49].

To determine the temporal response in the RelA interactome of phosphorylated proteins to the different DNA damaging agents, we evaluated those quantified proteins exhibiting a statistically significant (*t*-test, $P \leq 0.05$) change in response to time-dependent treatment with ETO or HU, in comparison to control (DMSO treated) cells. Interestingly, the constituents of the RelA interactome changed very little in response to DNA damage, with the vast majority of the phosphoproteins identified being observed before and after exposure to either ETO or HU (round nodes, Figure 2). Of the 803 protein binding partners with high confidence interactors, only 7 were unique to ETO (diamond nodes, Figure 2; Table 1), while 8 were specific to HU (square nodes, Figure 2; Table 1).

Of the 7 ETO-specific proteins identified in this network, three are essential components of the ERK/MAPK signalling pathway: the protein kinases ERK1 and PAK, and DUSP9, a dual specificity phosphatase that

Biochemical Journal (2021) **478** 533–551
https://doi.org/10.1042/BCJ20200627

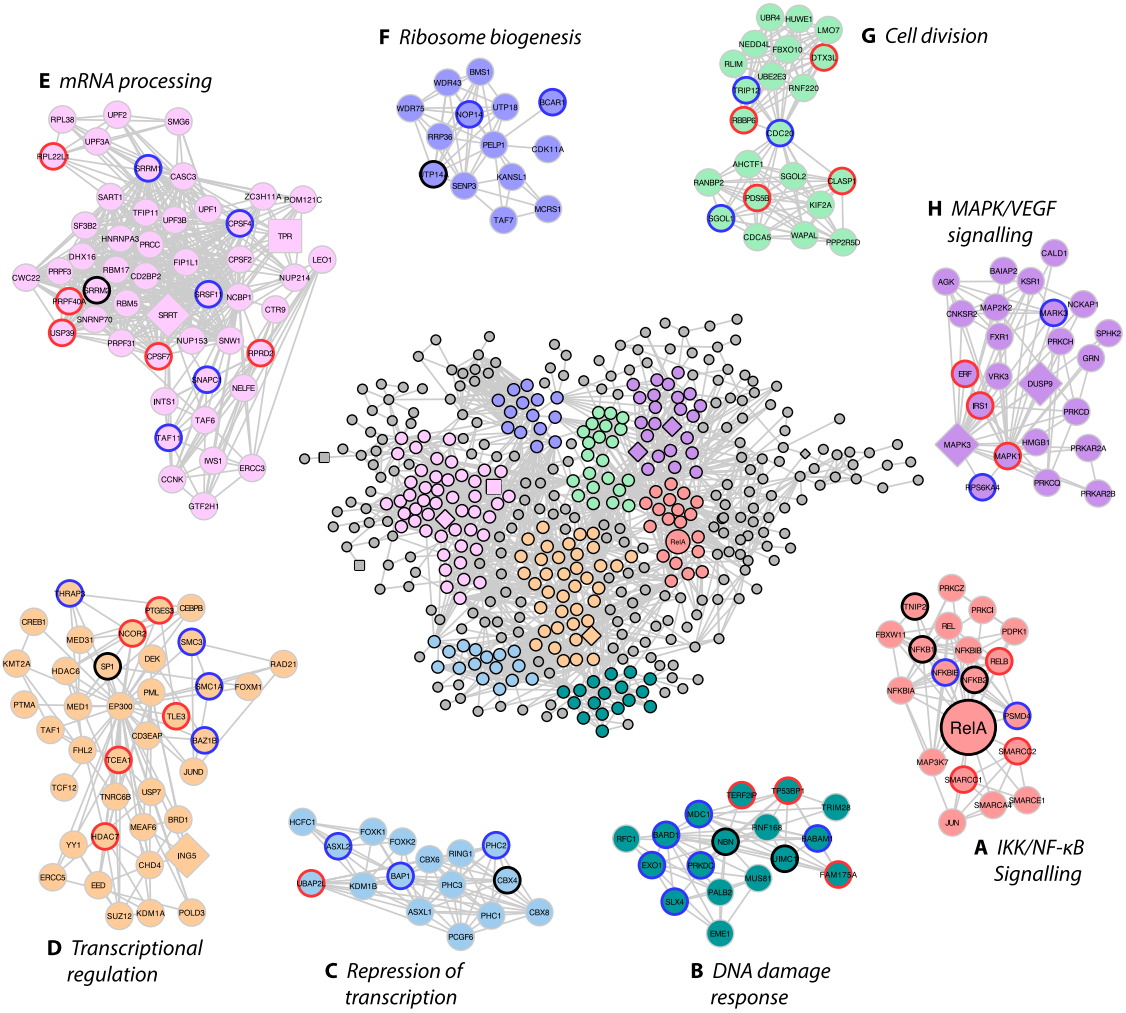

Figure 2. Network map of RelA interacting phosphoproteins.

Proteins from phosphopeptides quantified following HA-RelA immunoprecipitation in control (0.1% DMSO), ETO (50 μM) or HU (2 mM) treated U2OS cells were evaluated with STRING (v11.0) [35] for prior experimental evidence of interaction. Kmeans clustering was used to identify the top 9 enriched GO clusters of biological function and plotted using Cytoscape [36]. The shape of the nodes represent the conditions under which they was identified: round nodes represents proteins identified across all conditions; diamond nodes indicate proteins unique to ETO treatment; square nodes indicate proteins unique to HU treatment. (**A**) red nodes represent those proteins mapped to IKK/NF-κB signalling; (**B**) dark green nodes represent those proteins mapped to DNA damage response/DNA repair; (**C**) blue nodes represent those proteins mapped to repression of gene expression; (**D**) yellow nodes represent those proteins mapped to transcriptional regulation; (**E**) pink nodes represent those proteins mapped to mRNA processing/splicing; (**F**) violet nodes represent those proteins mapped to ribosome biogenesis/rRNA processing; (**G**) light green nodes represent those proteins mapped to cell division/mitosis; (**H**) purple nodes represent those proteins mapped to MAPK/VEGF signalling. Proteins outside of these eight enriched clusters have nodes in grey. The outline colour of the nodes within the eight clusters shows proteins with differentially regulated phosphopeptides following treatment with either ETO (blue), HU (red), or both (black).

preferentially targets the MAPK/ERK family. A fourth member of this ETO-specific cohort, AAED1 (which has no known common confident interactors and is therefore not represented in Figure 2), is also reported to positively regulate the ERK/MAPK (and AKT1) pathway, ultimately leading to upregulation of hypoxia-inducible factor (HIF)-1α and enhanced glycolysis [50]. In contrast, the 8 HU-specific proteins exhibited diverse biological functions, with only one of these proteins, nucleoprotein TPR, falling into one of the top 8 network clusters (Figure 2A).

Biochemical Journal (2021) **478** 533–551
https://doi.org/10.1042/BCJ20200627

Table 1 DNA damage specific RelA binding partners

Treatment	UniProt ID	Protein name
Etoposide	Q86U06	Probable RNA-binding protein 23
	O96013	Serine/threonine-protein kinase PAK 4
	P27361	Mitogen-activated protein kinase 3
	Q8WYH8	Inhibitor of growth protein 5
	Q9BXP5	Serrate RNA effector molecule homolog
	Q7RTV5	Peroxiredoxin-like 2C
	Q99956	Dual specificity protein phosphatase 9
Hydroxyurea	Q9BY44	Eukaryotic translation initiation factor 2A
	Q8N3F8	MICAL-like protein 1
	Q4G0J3	La-related protein 7
	O94979	Protein transport protein Sec31A
	Q12931	Heat shock protein 75 kDa, mitochondrial
	E9PRG8	Uncharacterized protein C11orf98
	O75113	NEDD4-binding protein 1
	P12270	Nucleoprotein TPR

Proteins identified as binding HA-RelA only in the presence of either etoposide or hydroxyurea are listed.

In support of the RelA protein networks defined in these proteomics experiments, we confirmed PAK4 as a novel ETO-regulated RelA binding partner by co-immunoprecipitation, with PAK4 binding occurring maximally in these experiments after 60 min treatment with ETO (Figure 3). No discernible increase in PAK4 binding was observed in response to cellular treatment with HU.

Also highlighted in the nodes of the top 8 network clusters are the proteins for which we identified statistically significantly differentially regulated phosphopeptides (*t*-test, $P \leq 0.05$) in response to treatment with either ETO or HU (or both) with respect to the (DMSO treated) control cells (Figure 2A–H; Supplementary Table S3). Interestingly, the proteins with differentially regulated phosphopeptides following either ETO or HU treatment are largely distinct between the two types of DNA damaging agents, and are interspersed across the network clusters rather than being specific to certain functional biological groups (Supplementary Figure S2-gifs). These data thus suggest that whilst there was relatively little change in the RelA-associated

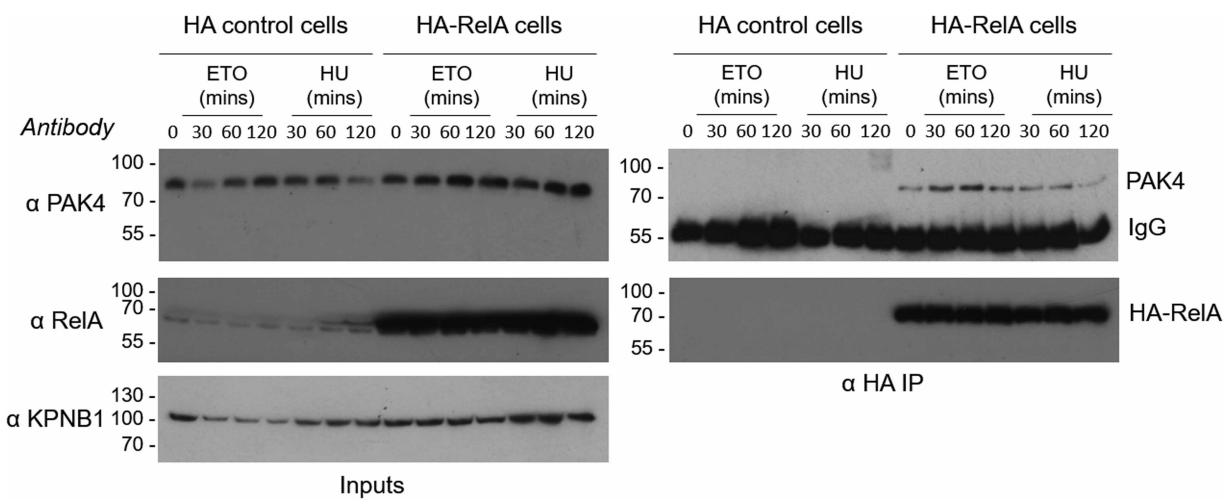

Figure 3. Co-immunoprecipitation of PAK4 with RelA increases following cellular treatment with etoposide.
HA-RelA or HA control U2OS cells were treated with either ETO (50 μM) or HU (2 mM) for the times indicated to induce DNA damage. Total cell extracts (inputs, left) or HA-RelA immunoprecipitated samples (αHA IP, right) were then analysed by western blot with antibodies against either PAK4, RelA or KPNB1 (as a loading control). Data are representative of three independent experiments.

phosphoproteins as a function of DNA damage, the phosphorylation states of those associated proteins were dependent on both the type and duration of the induced DNA damage response.

Rela is minimally differentially phosphorylated in U2OS cells in response to ETO or HU treatment

Looking specifically at RelA, we observed good sequence coverage of the N-terminal region (>70%; 46% overall; Supplementary Fig. S3), allowing us to quantify most of the known phosphorylation sites in the N-terminal half of the protein including; Ser42, Ser45, Ser131, Ser203/Ser205, Ser238, Ser240 and S316. Two novel phosphorylation sites at Thr54 and Ser169 were also observed (Supplementary Fig. S3). No phosphorylation sites were confidently identified in the *C*-terminus of RelA containing the transactivation domains (TAs), in part due to the limited ability to generate suitable tryptic peptides for analysis (as documented previously [26]). Although phosphopeptides covering the extreme *C*-terminus (from residue 503 and including the known sites of phosphorylation at T505, S529 and S536) were observed, the site of phosphorylation could not be unambiguously defined.

Overall, the changes observed in RelA phosphorylation in response to DNA damage under these conditions were very limited. Only Ser131 was statistically significantly regulated by both the DSB-inducing ETO and HU: pSer131 increased marginally by 1.03-fold (with respect to the DMSO-treated control) at 120 min (P-value = 0.047) in response to ETO, responding more rapidly to HU, increasing 1.05 fold by 30 min (P-value = 0.046), decreasing slightly (although not statistically) by 60 min, and returning to baseline levels by 120 min. We have previously shown that this site is also responsive to TNFα treatment of U2OS cells, and phosphorylated *in vitro* by IKKβ, in a manner that is significantly enhanced in the presence of the RelA dimerization partner, p50, and reduced in the presence of IκBα [26]. In contrast, Ser45, a phosphorylation site that we previously demonstrated plays a critical role in reducing the ability of RelA to bind to DNA (alongside Ser42, which was not observed in the HU-treated cells) [26], was reduced by 1.1 fold (P-value <0.01) 60 min after cellular treatment with HU, suggesting an HU-mediated regulation of RelA transcription, in part through Ser45 phosphorylation (Supplementary Fig. S3).

ETO and HU induced different phosphorylation dynamics in the RelA network

Of the 696 proteins identified in the RelA network in the presence of ETO, 184 exhibited ETO-dependent changes in phosphorylation status, with a total of 312 phosphopeptides exhibiting a statistically significant change. GO term analysis of biological processes of these 184 proteins revealed enrichment primarily of proteins involved in transcription ($P < 0.001$), RNA processing ($P < 0.001$), cell division ($P < 0.001$) and, unsurprisingly, the DNA damage response ($P < 0.001$) (Figure 4A). Slightly fewer changes arose in response to HU, with 235 phosphopeptides from 157 proteins exhibiting a statistically significantly change compared to control (Figure 4B), those primarily being involved in translation ($P < 0.001$) and rRNA processing ($P < 0.001$). Interestingly, only 37 of the proteins exhibiting dynamic changes in response to treatment were common between the two types of DNA damaging agent, indicating significant differences in the mechanisms whereby RelA mediates the outputs from these two DNA damaging agents (Figure 4C). For each of the phosphorylation sites identified in these experiments, we also determined if they had been observed previously in either PhosphositePlus (PSP), or Peptide Atlas (PA), categorising our quantified phosphosites based on the number of prior observations (Supplementary Tables S2, S3). Of the ∼3100 unique phosphorylation sites identified in these studies, ∼70% have been previously observed at medium or high confidence in PSP, having been observed at least twice previously. Of those phosphorylation sites that were dynamically regulated (with statistical significance) in response to cellular treatment with either of these DNA damage agents, 86% and 93% (for ETO and HU respectively) have been reported previously.

We next evaluated the temporal dynamics of these phosphorylation changes as a function of treatment type (Figure 4D). Intriguingly, ETO and HU induced very different dynamics in phosphosite regulation. Indeed, approximately one-quarter (∼70 phosphopeptides) of the ETO-regulated phosphopeptides, were responsive within 60 min of treatment, with the change in phosphorylation status being maintained over the duration of the 120 min experiment (Figure 4D,E). In contrast, only 8% (∼20 phosphopeptides) of HU-dependent phosphorylation changes occurred within the first 60 min and were then sustained for the duration (Figure 4D,F). Overall, HU-mediated phosphorylation changes were much more dynamic, with 39% of the phosphopeptides quantified in these experiments significantly regulated (being observed at either increased, or reduced levels), before reverting back, either to control levels, or in some instances, in the opposite direction. Just over half of

Biochemical Journal (2021) **478** 533–551
https://doi.org/10.1042/BCJ20200627

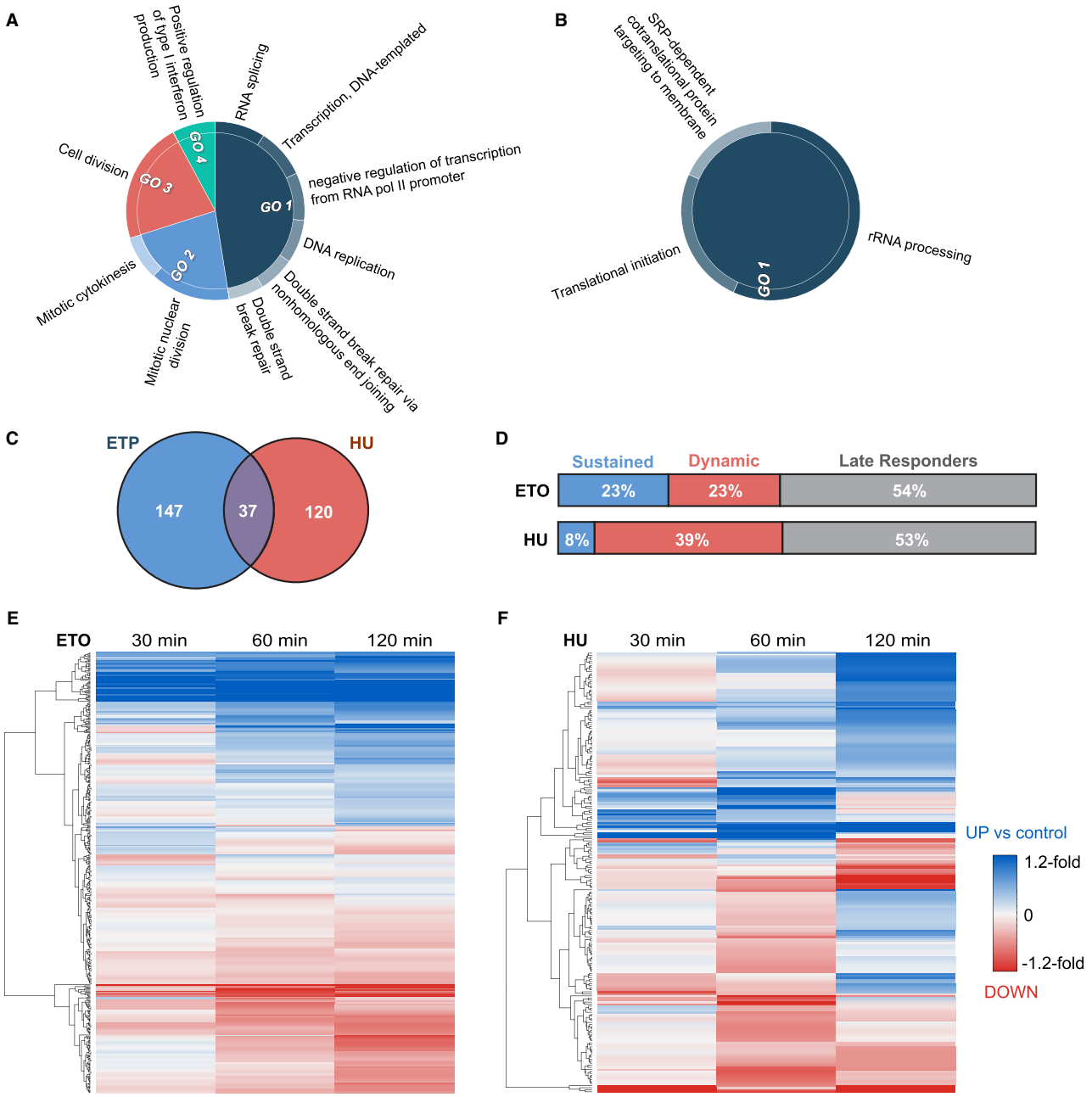

Figure 4. Etoposide and Hydroxyurea induced different phosphorylation dynamics in the RelA network.

GO term biological process enrichment was examined for all phosphopeptides exhibiting a statistically significant change in response to either (**A**) etoposide (ETO) or (**B**) hydroxyurea (HU). (**C**) Overlap of those proteins with significant change in phosphopeptide abundance at one or more time points with ETO or HU. (**D**) Distribution of phosphopeptide changes between sustained, dynamic and late responders for ETO vs HU treatment, where 'Late Responders' indicates a change at 120 min only, 'Sustained' indicates a change at 30 or 60 min which is sustained throughout, and 'Dynamic' indicates a change at 30 or 60 min which is reversed. (**E** and **F**) Heatmaps of the fold change in phosphopeptide levels following treatment with either ETO (**E**) or HU (**F**) at 30, 60 or 120 min relative to control levels. Hierarchical row clustering was performed on the $\log_2$ fold changes.

those phosphopeptides that were differentially regulated by either ETO or HU did not exhibit a statistically significant change until after more than 60 min of continuous treatment, i.e. they were late responders that were only observed in these experiments 120 min after exposure (Figure 4D).

Phosphorylation of RelA-associated proteins in response to etoposide

Of the 312 phosphopeptides that were differentially regulated by ETO (with respect to the untreated control ($P \leq 0.05$)) across all time-points, 151 increased in abundance, while 159 were down-regulated (Supplementary Table S2). Only two phosphorylation sites exhibited significant temporal dynamics (with levels being significantly elevated or decreased at sequential time-points), although the selective nature of the timing at which these measurements were made could be masking additional dynamics. Overall, the relative fold change in phosphopeptide abundance (up- or down-) was relatively small, with the greatest statistically significant fold change being ∼1.4 (Figure 5A–C; Supplementary Table S2). 14 phosphopeptides were quantified in all three biological replicates for a given ETO condition but absent in control cell lysates. As the fold-change in relative abundance could thus not be defined for these phosphopeptides, they are not represented on the volcano plots in Figure 5A.

In-depth functional enrichment analysis of proteins that were either up- or down-regulated following ETO exposure revealed some key differences in terms of the biological functions that were regulated (Figure 5D). RelA-associated proteins with an ETO-mediated reduction in phosphopeptide levels showed significant enrichment for GO terms including mitosis, chromatin regulation (including H4-K16 acetylation), transcriptional regulation and DNA damage repair (Figure 5D). pSer780 on MDC1, the Mediator of DNA damage checkpoint protein 1, exhibited the greatest down-regulation of all phosphosites in response to ETO across the time-points investigated (1.3-fold down; $P = 1.95 \times 10^{-04}$) (Supplementary Table S2, Figure 5A–C). This phosphorylation site has previously been identified has being induced in response to ionising radiation (IR) [51] and ultraviolet (UV) radiation [52], both of which induce DSB, although the physiological function of this phosphorylation site has not yet been defined. We show here that the proportion of Ser780 phosphorylated MDC1 that contributes to the RelA interactome decreases in response to ETO, suggesting that DNA-damage induced pSer780 may serve to disrupt the interaction of MDC1 with RelA transcriptional complexes.

It is interesting to note that many more phosphopeptides were significantly upregulated than were decreased in the RelA interactome in response to ETO, particularly in the later time points. Transcriptional regulation and DNA damage repair were also among the GO terms enriched for those proteins with up-regulated phosphorylation sites. However, there was only an ∼8% overlap in common proteins with differentially regulated (up or down in response to ETO) phosphopeptides (Supplementary Table S2), suggesting co-ordinated regulation of these key processes largely through different protein effectors rather than differential phosphorylation-mediated regulation of the same proteins. Also among the GO terms enriched in the list of proteins with up-regulated phosphopeptides in response to ETO were mRNA processing, ATP binding, transcription corepressor functionality and type I interferon production, including the NF-κB signalling proteins (RelA (pSer131), NFKB1 (p105/p50) (pSer923;Ser927) and NFKB2 (p100/p52) (pSer858, pTyr868 and pSer870), with pSer619 on the RNA helicase DDX41 and pSer3205 on the DNA-dependent protein kinase PRKDC (Figure 5D). Multiple phosphopeptides from the transcription factor zinc finger protein 281 (ZNF281/GZP1/ZBP99), containing pSer395 ($P = 2.1 \times 10^{-02}$), pSer620 ($P = 1.1 \times 10^{-04}$), pSer785 ($P = 1.9 \times 10^{-06}$) and pSer807 ($P = 1.7 \times 10^{-03}$), were significantly upregulated across all time points (between 1.2–1.4-fold) in the RelA interactome in response to ETO, but not in response to HU. ZNF281 has recently been reported to be recruited to DSBs, following interaction of its zinc finger domain with XXCR4 [53], where is plays an important role in non-homologous end-joining upon DNA damage, and consequently the maintenance of cell viability. Supporting our observations of increased phosphopeptides in response to DSB, these authors also reported a slight reduction in the recruitment of a non-phosphorylatable S785A/S807A ZNF281mutant to sites of DNA damage. Based on our data, we would suggest that phosphorylation of ZNF281 on Ser395 and Ser620 may also be required for its optimal recruitment to DNA lesions and subsequent DNA repair.

In an attempt to understand the signalling pathways and possible kinase-substrate relationships feeding into the ETO-dependent changes in phosphorylation of the RelA-binding partners, the 'class I' localized phosphosites (ptmRS ≥ 0.75) with P-value ≤0.05 were used as input sequences for the NetPhorest kinase-substrate prediction algorithm [34,35] (Figure 5E). Of the 117 down-regulated and 107 up-regulated phosphorylation sites that passed the above thresholds, NetPhorest gave kinase-substrate predictions for 37 and 32 sites respectively. Among the down-regulated sites, the CDKs had the highest number of predicted substrates (14, 38%), accounting at least partially, for the notable enrichment across all the ETO down-regulated phosphorylation sites for Pro in the +1 position with respect to the site of phosphorylation [54] (Figure 5F). Although CDK1 was defined by NetPhorest as the most likely regulator of these substrates (Supplementary Table S2 and Figure 5), it

Biochemical Journal (2021) **478** 533–551
https://doi.org/10.1042/BCJ20200627

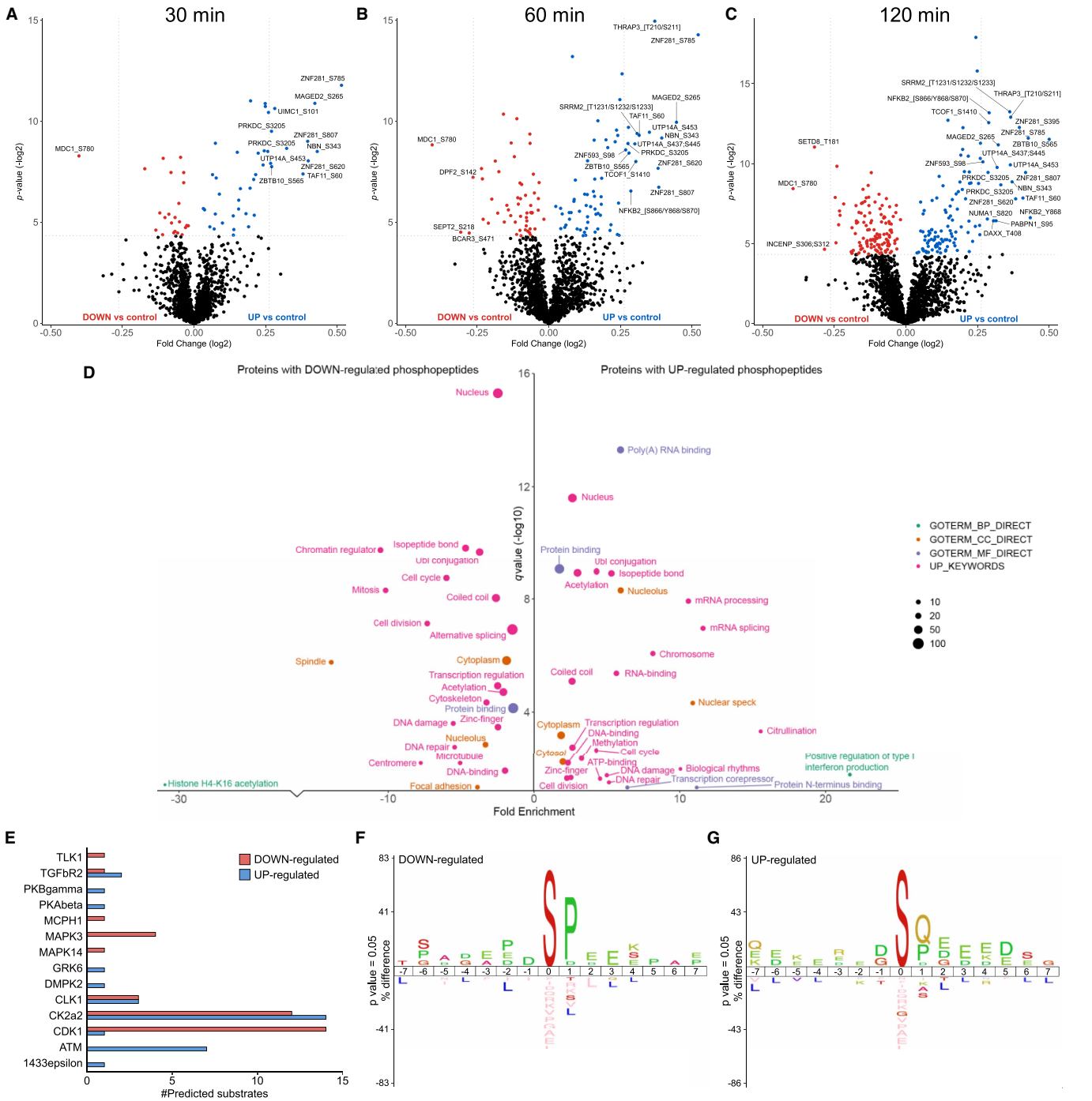

Figure 5. Etoposide-mediated phosphopeptides changes in the RelA network.

Volcano plots showing fold changes in phosphopeptide abundance following Bayesian statistical analysis to evaluate significant differences as a function of (**A**) 30 min, (**B**) 60 min or (**C**) 120 min treatment with ETO. Log_2-fold change are presented as a function of the $-Log_2$ p-value; differentially down-regulated (red) or up-regulated (blue) phosphopeptides with a *P*-value ≤0.05 are highlighted. Select data points are annotated with their protein accession number and site of phosphorylation. Phosphopeptides observed upon ETO treatment, but not in the control extracts are not reported here. (**D**) GO term enrichment analysis using DAVID of proteins with significantly regulated phosphopeptides in response to ETO (all time points) relative to control. Phosphopeptides with a Benjamini–Hochberg adjusted *P*-value ≤0.05 are labelled. BP, biological process (green); CC, cellular compartment (yellow); MF, molecular function (purple); UP, UniProt keyword (pink). (**E**) NetPhorest kinase-substrate prediction for significantly down- (red) or up-regulated (blue) phosphosites. IceLogo sequence analysis of (**F**) down-regulated or (**G**) up-regulated phosphosites.

should be noted that the overlapping substrate specificity of CDK1/2/3/5 means that it is not possible to differentiate substrates of the different CDK family members. The identification of four predicted substrates for ERK1 (MAPK3), which is also a Pro-directed protein kinase [55], likely also contributes to the identified sequence motif, and correlates with our observations of this enzyme, and importantly, a cognate phosphatase, DUSP9, in the RelA network under these conditions.

IceLogo sequence analysis of the ETO up-regulated phosphosites showed significant enrichment for Gln (and to a lesser extent Pro) at the +1 position with respect to the site of phosphorylation (Figure 5G). Positions +2 to +5 also exhibited a strong preference for acidic residues (Asp/Glu), consistent with observation of 14 predicted substrates for casein kinase II alpha (CK2α2) in the NetPhorest output (Figure 5E). Perhaps not surprisingly given its somewhat promiscuous substrate repertoire, and an involvement in diverse cellular processes (including regulation of numerous transcription factors such as NF-κB), CK2α2 was also predicted as the regulatory enzyme for a number of the significantly down-regulated phosphorylation sites. The striking observation of Gln at +1 in 36 of the up-regulated phosphorylation sites (Figure 5G) is in agreement with previous reports of ATM/ATR-dependent regulation of the RelA NF-κB pathway in response to DSB (albeit following cellular exposure to TNFα rather than etoposide) [56]. ATM/ATR kinases are well known to preferentially phosphorylate Ser/Thr residues followed by a Gln, with substrates often containing several closely spaced SQ/TQ motifs in regions termed SQ/TQ cluster domains (SCDs) [57]. Whilst just 7 of the 36 SQ motif-containing sequences were predicted by NetPhorest to be ATM sites, it is possible that many more of the differentially regulated phosphosites that match to this consensus are potential ATM/ATR substrates, given the limitations of prediction software. While phosphorylation at any given site can be induced by more than one protein kinase in cells, the NetPhorest algorithm is best used as a guide and will only assign a single potential enzyme, based on the best fit, and is therefore not fully representative of cellular possibilities.

Phosphorylation of RelA-associated proteins in response to hydroxyurea

Upon HU treatment, 235 phosphopeptides from 157 proteins in the RelA interactome network were significantly differentially regulated with respect to the DMSO treated control ($P \leq 0.05$; Figure 6A–C). Of those, 121 phosphopeptides increased in abundance, while levels reduced for 109 phosphopeptides. Among the phosphorylation sites exhibiting a dynamic response over the time-course of HU treatment, five showed a bi-directional response, increasing in some time points, but reducing in others, with respect to control levels (Supplementary Table S3). Only seven phosphopeptides were quantified in all three biological replicates at a single HU time point that were not observed in the control cell extracts.

RelA-associated proteins with statistically significantly reduced phosphopeptide levels in response to HU-mediated DNA damage were notably enriched for GO terms encompassing ribosome biogenesis, mRNA processing and translation (Figure 6D). Notably, whilst translation was enriched among the proteins effected by HU treatment there was no significant enrichment for proteins involved in translation with ETO. In contrast, elevated phosphopeptide levels were observed for processes such as chromatin regulation and chromosomal rearrangement, and to a lesser extent, transcriptional regulation and mitosis (Figure 6D). Whilst transcriptional regulation was among the GO terms enriched in response to HU, it was only marginally enriched, and with a much lower significance than our observations with ETO, suggestion a more much limited effect on transcriptional regulation with HU than with ETO (Figure 5D, Figure 6D).

In agreement with the γH2Ax immunoblotting data (Figure 1B) which indicated a slower cellular response to HU than ETO (see the heatmaps in Figure 4F), very few significant changes in phosphopeptide abundance were observed 30 min after treatment with HU (Figure 6A). Interestingly, the NFKB2 (p100) peptide phosphorylated on either Ser858/Thr859 (site ambiguous) exhibited the greatest increase of any phosphopeptides at this time point, with a 1.4-fold change (Supplementary Table S3; being observed in two charge states) (Figure 6B). This increase in HU-mediated phosphorylation is supported by additional quantification of a smaller peptide in which the site of phosphorylation was defined as Ser858 (Supplementary Table S3), a site which was also significantly upregulated following exposure to ETO (Supplementary Table S2). Of note, these peptides (and others in the C-terminus of p100 that are differentially regulated in response to treatment) are specific to p100, rather than the transcriptionally active p52 cleavage product, suggesting DNA damage-mediated regulation of either p100 processing, or its ability to bind (directly or indirectly) to RelA.

The second most differentially elevated phosphopeptide after 30 (and 60) min treatment with HU was the doubly phosphorylated pThr185/pTyr187-containing peptide from ERK2. This phosphopeptide lies in the kinase activation loop and phosphorylation of both of these sites is required for catalytic activation of ERK2

PORTLAND PRESS

Biochemical Journal (2021) **478** 533–551
https://doi.org/10.1042/BCJ20200627

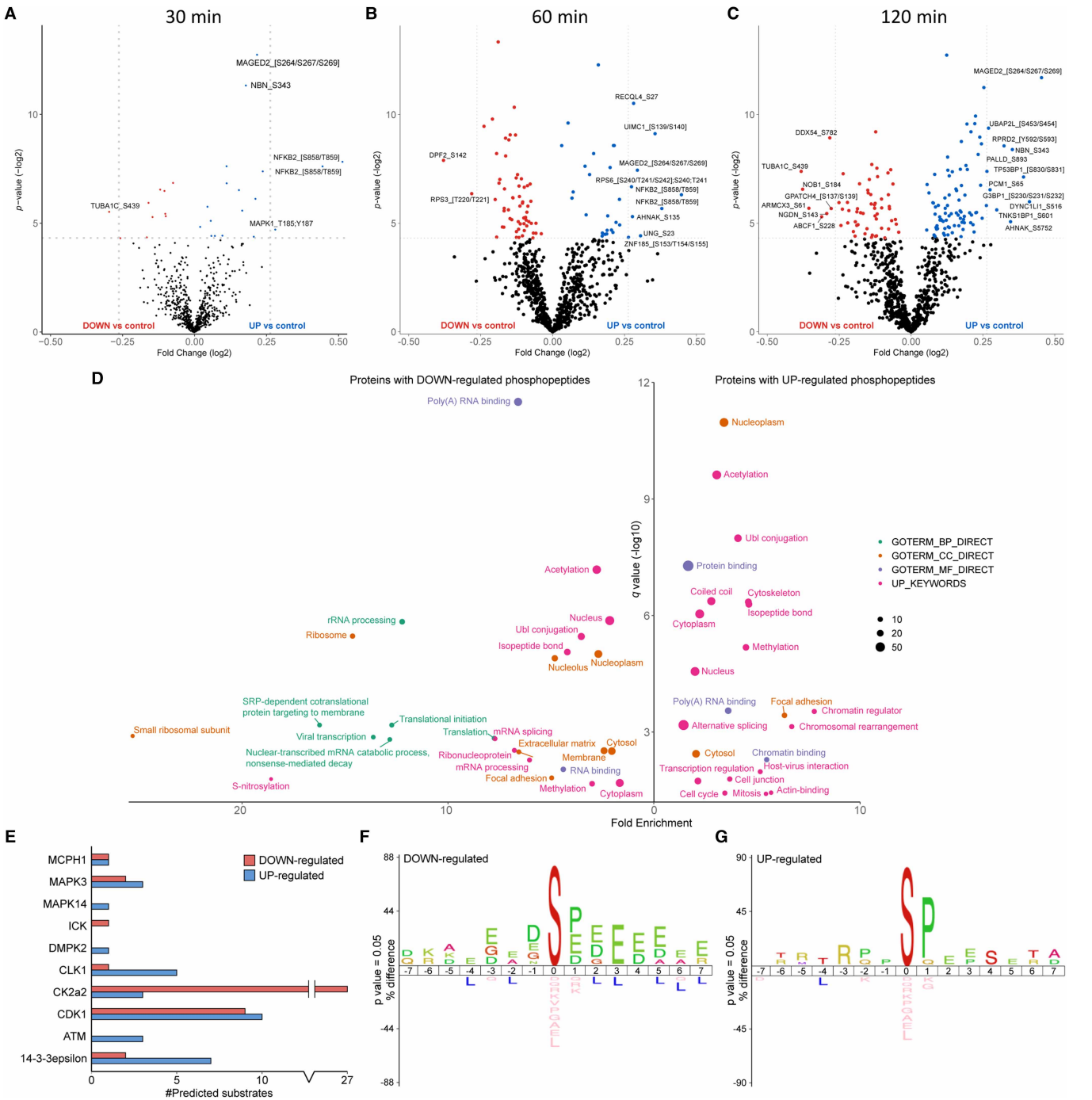

Figure 6. Hydroxyurea-mediated phosphopeptides changes in the RelA network.

Volcano plots showing fold changes in phosphopeptide abundance following Bayesian statistical analysis to evaluate significant differences as a function of (**A**) 30 min, (**B**) 60 min or (**C**) 120 min treatment with HU. Log_2-fold change are presented as a function of the $-Log_2$ p-value; differentially down-regulated (red) or up-regulated (blue) phosphopeptides with a *P*-value ≤0.05 are highlighted. Select data points are annotated with their protein accession number and site of phosphorylation. Phosphopeptides observed upon HU treatment, but not in the control extracts are not reported here. (**D**) GO term enrichment analysis using DAVID of proteins with significantly regulated phosphopeptides in response to HU (all time points) relative to control. Phosphopeptides with a Benjamini–Hochberg adjusted *P*-value ≤0.05 are labelled. BP, biological process (green); CC, cellular compartment (yellow); MF, molecular function (purple); UP, UniProt keyword (pink). (**E**) NetPhorest kinase-substrate prediction for significantly down- (red) or up-regulated (blue) phosphosites. IceLogo sequence analysis of (**F**) down-regulated or (**G**) up-regulated phosphosites.

[58,59]. An early consequence of HU treatment on the RelA interactome network thus appears to be activation of bound ERK2, which contrasts with our observations with ETO, where there were no significant changes induced in MAPK1/ERK2 phosphopeptides. These findings are curious in light of the fact that the C-terminal region of p100 is reported to bind to inactive ERK2, thereby preventing its phosphorylation and nuclear translocation. The fact that we observe increased phosphorylation of ERK2 alongside phosphorylation in the C-terminal 'death domain' of p100 may suggest a role for these p100 phosphorylation sites in regulating its ability to interact with ERK2 [60].

Nibrin, a member of the MRN complex which plays a critical role in DSB repair and cell cycle checkpoint control, also exhibited elevated Ser343 phosphorylation by 30 min HU treatment. Interestingly, the pSer343 site observed falls within an SQ motif which has previously been shown to be phosphorylated by ATM in response to IR, and is believed to play a role in intra-S phase checkpoint activation [61,62] (Figure 6A,E). This same phosphorylation site was also rapidly elevated in response to ETO (Figure 5B), confirming its apparent involvement in a generic ATM-mediated DNA damage response [61,62]. By 60 min, we also observed reduced levels of pSer142 on DPF2 (Zinc finger protein ubi-d4), a known regulator of the non-canonical NF-κB pathway [63], and pThr220/221 (site ambiguous) on the RelA binding partner RPS3 (40S ribosomal protein S3), both of which have previously been reported to be elevated in HEK293 cells following 3 h UV exposure [52]. Although binding of RSP3 to RelA is thought to enhance its ability to bind DNA *in vitro* [64], RSP3 functions as a negative regulator of H_2O_2-mediated DNA repair [65]. It is possible therefore that pThr220/221 on RPS3, and pSer142 on DPF2, serve to modulate the RelA transcriptional complexes and/or the consensus promoter regions for NF-κB binding, that are required for DNA repair in response to HU.

Using NetPhorest [41,42], we were able to predict possible kinase-substrate relationships for 46% (77 out of 167) of the 'class I' phosphosites (*ptm*RS ≥ 0.75) that were regulated in response to HU (Figure 6E). CK2α2 was predicted as the kinase responsible for the vast majority (27 out of 43) of the phosphosites reduced in response to HU, based on the prevalence of acidic residues C-terminal to the site of phosphorylation (in particular at +3) clearly evident in the sequence analysis (Figure 6F). Consequently, HU might have significant effects on CK2α2 (or other acidophilic kinases) that feed into the RelA-mediated DNA damage response. Prevalent among both up- and down-regulated phosphosites were predicted substrates of the cyclin-dependent kinases (CDK1/2/3/5 group) which, together with the prediction of substrates for ERK1 (MAPK3) and p38α (MAPK14), contributes to the enrichment of Pro at the +1 position in both the HU up- and down-regulated phosphosites (Figures 5G, 6F). Also among the up-regulated phosphopeptides are a number of predicted ATM substrates which, whilst only representing a small proportion of the total number of HU-regulated phosphosites, corresponds with the small enrichment for Gln in the +1 position among the up-regulated phosphosites. (Figure 6E,G).

Comparing the putative kinase-mediated regulation of substrates for those differentially regulated phosphopeptides in the RelA interactome in response to the two different types of DNA damaging agents revealed some interesting observations: although ATM-predicted substrates were enhanced with both ETO and HU, over twice as many putative substrates were elevated with ETO. Predicted substrates for CK2α2 are prevalent in the differentially regulated (both up- and down-) phosphosites under both conditions, although HU induces a far greater reduction in levels of putative CK2α2 substrates than ETO. In contrast, putative substrates for the dual specificity protein kinase CLK1, which has a role in regulating alternative splicing, are notably elevated in response to HU (Figure 6E), but not particularly with ETO (Figure 5E). Interestingly, binding sites for 14-3-3ε, which generally conform to the RXXpS/TXP consensus, were elevated under both conditions, but particularly in response to HU. 14-3-3 proteins are known to be involved in the cellular response to DNA damage; 14-3-3ε in particular modulates NF-κB signalling in part by virtue of its ability to bind phosphorylated TAK1 (and its cognate phosphatase PPM1B), and thereby regulate its anti-apoptotic capabilities [66,67]. In response to DNA damage stress, this manifests as inhibition of the anti-apoptotic activity of TAK1, promoting an apoptotic phenotype that is enhanced by the 14-3-3ε-mediated disruption of DP-2 from the E2F transcriptional complex [68]. The fact that we observe elevated putative 14-3-3ε binding sites following HU treatment (but significantly less so with ETO), is in agreement with the pro-apoptotic response of HU-treated cells. Consequently, we hypothesise that the ability of components of the RelA interactome to bind 14-3-3ε may be a driving factor in achieving the expected cell death/survival phenotype in response to these two DNA damaging agents.

Discussion

Protein phosphorylation is a key reversible, dynamic PTM that rapidly governs protein complex formation, particularly of transcription factor complexes, thereby coupling extracellular stressors with compensatory

Biochemical Journal (2021) **478** 533–551
https://doi.org/10.1042/BCJ20200627

transcriptional output. To understand the role of phosphorylation in regulating the RelA transcriptional network in response to different types of DNA damage, we used quantitative phosphoproteomics to explore the dynamics of the phosphorylated RelA interactome in response to either ETO or HU. Evaluating the RelA network under these conditions is pertinent, given the central role of this transcription factor in directing the cellular response towards either senescence or apoptosis. Exposure of U2OS cells to either ETO or HU had very limited effect on the phosphorylated RelA interactome; only 246 of the 815 RelA interacting phosphoproteins that we identified in total changed upon treatment. Of these, less than 1% were specific to the type of DNA stress, with 7 or 8 unique proteins (respectively) being identified in the RelA network following exposure of U2OS cells to either the DSB-inducing ETO or to HU. However, although there was little change in the make-up of this network, there was evidence of subtle, but significant, changes in the phosphorylation states of the RelA bound proteins as a function of both the type of and duration of the DNA damaging agent used. Not only did the anti-apoptotic agent ETO invoke a more rapid cellular response than HU, both in terms of maximal H2AX levels (Figure 1B), and quantifiable changes in phosphopeptide levels (Figs. 4–6; Supplementary Tables S2, S3), but interestingly this study pointed to the differential regulation of key cellular processes and the involvement of unique signalling pathways in modulating the treatment-specific functions of RelA.

Examination of the RelA network hub (the bait) revealed two novel phosphorylation events amongst the RelA phosphopeptides that we were able to identify and quantify in this trypsin-based peptide analysis: Thr54 and Ser169, both of which are within the DNA binding domain. However, only Ser45 and Ser131 were statistically differentially regulated in response to either ETO or HU. While Ser131 was statistically elevated upon treatment with ETO at 120 min, the fold change was marginal (1.03-fold), with similar fold change (1.05-fold) being observed for this phosphosite in response to HU, albeit at a shorter 30 min time point. The RelA peptide containing pSer45 was unchanged upon ETO treatment, and was statistically down-regulated by 60 min exposure to HU, again with low (1.05) fold change. Given that we were evaluating the total cellular pool of RelA, rather than specifically the nuclear portion where we would expect e.g. Ser45 phosphorylation to have a greater regulatory effect [26], it is perhaps not surprising that the phosphopeptide changes quantified in this study were low.

A number of our findings of regulated phosphorylation site changes are in agreement with other published studies. However, the overall fold change in phosphopeptide levels across this study were relatively small (maximally 1.7 fold), and speaks to the necessity to avoid, wherever possible, implementation of a fold-change cut-off during this type of analysis. While ETO-regulated RelA bound phosphoproteins were primarily involved in transcription, cell division and mitosis, and DSB repair (as might be expected), HU-mediated changes were predominantly observed in proteins with functions in rRNA and mRNA processing, and translational initiation. Where changes were observed, ETO predominantly resulted in elevated phosphopeptide levels, with a number of the ETO-regulated phosphorylation sites identified having been reported previously to be modulated in response to either IR or UV radiation. It was interesting to note that transcriptional regulation and DNA damage repair proteins were enriched in those datasets with both elevated and reduced phosphopeptide levels, suggesting coordinated regulation of these processes through different effectors in response to DSB. In addition to the involvement in AMT/ATR signalling previously reported, potential substrates for which were much more prevalent following ETO treatment that HU, kinase substrate prediction suggested roles for CDKs and ERK1 (or their cognate phosphatases), in regulating RelA complexes in response to ETO. In contrast, levels of the activation loop phosphopeptide in MAPK1/ERK2, traditionally thought to be a marker of kinase activity, were elevated in response to HU, but not ETO, suggesting differential MAPK isoform signalling in response to these two types of DNA damage. The prediction of substrates for p38α in the regulated phosphorylation sites following cellular exposure to HU (but not ETO), also points to a potential HU-specific regulation of this stress activated protein kinase. Finally, our data point to a role for 14-3-3ε binding propensity in facilitating the cellular response to HU, which may be a contributing factor in differentiating the pro-and anti-apopotic phenotypes that are the result of prolonged cellular expose to these two types of DNA damaging agents, and we believe is worthy of further investigation.

Data Availability

The mass spectrometry proteomics data have been deposited to the ProteomeXchange Consortium via the PRIDE partner repository with the dataset identifiers PXD019587 and PXD019589.

Competing Interests

The authors declare that there are no competing interests associated with the manuscript.

Funding
This work was supported by the Biotechnology and Biological Sciences Research Council (BBSRC; BB/L009501/1 to C.E.E. and N.D.P., BB/R000182/1 and BB/M012557/1 to C.E.E.) and Cancer Research UK (CRUK; C1443/A22095 to N.D.P. and C.E.E., and C1443/A12750 to N.D.P.).

Open Access
Open access for this article was enabled by the participation of University of Liverpool in an all-inclusive *Read & Publish* pilot with Portland Press and the Biochemical Society under a transformative agreement with JISC.

Author Contributions
C.E.E. and N.D.P. obtained funding. A.C., C.F.F. and C.E.E. designed the experiments and analysed the data, with bioinformatics support from S.P., A.K. and A.R.J. L.S. generated the HA-RelA U2OS cell line. C.F.F. treated the cells, prepared the samples and did the immunoblotting studies. A.C., C.F.F. and P.J.B. performed the MS analysis. E.C. performed the RelA CoIPs. A.C. and C.E.E. wrote the paper with contributions from all authors, who also approved the final version prior to submission.

CRediT Contribution
Claire E. Eyers: Conceptualization, Formal analysis, Supervision, Funding acquisition, Visualization, Writing — original draft, Project administration, Writing — review and editing. **Amy E. Campbell:** Conceptualization, Data curation, Investigation, Visualization, Writing — original draft. **Caterina Ferraz Franco:** Conceptualization, Formal analysis, Investigation, Visualization, Writing — original draft. **Ling-I Su:** Methodology. **Emma K. Corbin:** Validation, Visualization. **Simon Perkins:** Data curation, Software. **Anton Kalyuzhnyy:** Data curation, Formal analysis. **Andrew R. Jones:** Data curation, Software, Supervision. **Philip J. Brownridge:** Resources, Data curation, Supervision, Investigation. **Neil D. Perkins:** Formal analysis, Supervision, Validation, Project administration, Writing — review and editing.

Abbreviations
AGC, automatic gain control; CID, collision-induced dissociation; DSB, double strand break; ETcaD, electron transfer with supplemental collision activation; ETD, electron-transfer dissociation; EThcD, electron-transfer higher energy collisional dissociation; ETO, etoposide; GO, gene ontology; HCD, higher energy collisional dissociation; HU, hydroxyurea; IR, ionizing radiation; MS, mass spectrometry; PD, Proteome Discoverer; PTM, post-translational modification; RHD, Rel homology domain; TD, transactivation domain; UV, ultraviolet.

References
1 Perkins, N.D. (2012) The diverse and complex roles of NF-κB subunits in cancer. *Nat. Rev. Cancer* **12**, 121–132 https://doi.org/10.1038/nrc3204
2 Christian, F., Smith, E. and Carmody, R. (2016) The regulation of NF-κB subunits by phosphorylation. *Cells* **5**, 12 https://doi.org/10.3390/cells5010012
3 Lu, X. and Yarbrough, W.G. (2015) Negative regulation of RelA phosphorylation: emerging players and their roles in cancer. *Cytokine Growth Factor Rev.* **26**, 7–13 https://doi.org/10.1016/j.cytogfr.2014.09.003
4 Giridharan, S. and Srinivasan, M. (2018) Mechanisms of NF-κB p65 and strategies for therapeutic manipulation. *J. Inflamm. Res.* **11**, 407–419 https://doi.org/10.2147/JIR.S140188
5 Kumar, A., Takada, Y., Boriek, A.M. and Aggarwal, B.B. (2004) Nuclear factor-κB: its role in health and disease. *J. Mol. Med.* **82**, 434–448 https://doi.org/10.1007/s00109-004-0555-y
6 Kim, H.J., Hawke, N. and Baldwin, A.S. (2006) NF-κB and IKK as therapeutic targets in cancer. *Cell Death Differ.* **13**, 738–747 https://doi.org/10.1038/sj.cdd.4401877
7 Didonato, J.A., Mercurio, F. and Karin, M. (2012) NF-κB and the link between inflammation and cancer. *Immunol. Rev.* **246**, 379–400 https://doi.org/10.1111/j.1600-065X.2012.01099.x
8 Tilstra, J.S., Niedernhofer, L.J., Paul, D., Tilstra, J.S., Robinson, A.R., Wang, J., et al. (2012) NF- k B inhibition delays DNA damage – induced senescence and aging in mice find the latest version: NF- κ B inhibition delays DNA damage – induced senescence and aging in mice. *J. Clin. Invest.* **122**, 2601–2612 https://doi.org/10.1172/JCI45785
9 Wang, J., Jacob, N.K., Ladner, K.J., Beg, A., Perko, J.D., Tanner, S.M. et al. (2009) Rela/p65 functions to maintain cellular senescence by regulating genomic stability and DNA repair. *EMBO Rep.* **10**, 1272–1278 https://doi.org/10.1038/embor.2009.197
10 Chien, Y., Scuoppo, C., Wang, X., Fang, X., Balgley, B., Bolden, J.E., et al. (2011) Control of the senescence-associated secretory phenotype by NF-κB promotes senescence and enhances chemosensitivity. *Genes Dev.* **25**, 2125–2136 https://doi.org/10.1101/gad.17276711
11 Slater, M.L. (1973) Effect of reversible inhibition of deoxyribonucleic acid synthesis on the yeast cell cycle. *J. Bacteriol.* **113**, 263–270 https://doi.org/10.1128/JB.113.1.263-270.1973
12 Krakoff, I.H., Brown, N.C. and Reichard, P. (1968) Inhibition reductase of ribonucleoside by hydroxyurea1 diphosphate. *Cancer Res* **28**, 1559–1565 PMID:4876978

Biochemical Journal (2021) **478** 533–551
https://doi.org/10.1042/BCJ20200627

13 Stauber, R.H., Knauer, S.K., Habtemichael, N., Bier, C., Unruhe, B., Weisheit, S., et al. (2012) A combination of a ribonucleotide reductase inhibitor and histone deacetylase inhibitors downregulates EGFR and triggers BIM-dependent apoptosis in head and neck cancer. *Oncotarget* **3**, 31–43 https://doi.org/10.18632/oncotarget.430
14 Murai, J. and Pommier, Y. (2019) Phosphatase 1 nuclear targeting subunit, a novel DNA repair partner of PARP1. *Cancer Res.* **79**, 2460–2461 https://doi.org/10.1158/0008-5472.CAN-19-0798
15 Krämer, O.H., Knauer, S.K., Zimmermann, D., Stauber, R.H. and Heinzel, T. (2008) Histone deacetylase inhibitors and hydroxyurea modulate the cell cycle and cooperatively induce apoptosis. *Oncogene* **27**, 732–740 https://doi.org/10.1038/sj.onc.1210677
16 Pommier, Y., Leo, E., Zhang, H. and Marchand, C. (2010) DNA topoisomerases and their poisoning by anticancer and antibacterial drugs. *Chem. Biol.* **17**, 421–433 https://doi.org/10.1016/j.chembiol.2010.04.012
17 Montecucco, A. and Biamonti, G. (2007) Cellular response to etoposide treatment. *Cancer Lett.* **252**, 9–18 https://doi.org/10.1016/j.canlet.2006.11.005
18 Montecucco, A., Zanetta, F. and Biamonti, G. (2015) Molecular mechanisms of etoposide. *EXCLI J.* **14**, 95–108 https://doi.org/10.17179/excli2015-561
19 Schäfer, C., Göder, A., Beyer, M., Kiweler, N., Mahendrarajah, N., Rauch, A., et al. (2017) Class I histone deacetylases regulate p53/NF-κB crosstalk in cancer cells. *Cell. Signal.* **29**, 218–225 https://doi.org/10.1016/j.cellsig.2016.11.002
20 Schneider, G., Henrich, A., Greiner, G., Wolf, V., Lovas, A., Wieczorek, M., et al. (2010) Cross talk between stimulated NF-κB and the tumor suppressor p53. *Oncogene* **29**, 2795–2806 https://doi.org/10.1038/onc.2010.46
21 Wagner, T., Kiweler, N., Wolff, K., Knauer, S.K., Brandl, A., Hemmerich, P. et al. (2015) Sumoylation of HDAC2 promotes NF-κB-dependent gene expression. *Oncotarget* **6**, 7123–7135 https://doi.org/10.18632/oncotarget.3344
22 Wu, Z.H. and Miyamoto, S. (2008) Induction of a pro-apoptotic ATM-NF-κB pathway and its repression by ATR in response to replication stress. *EMBO J.* **27**, 1963–1973 https://doi.org/10.1038/emboj.2008.127
23 Perkins, N.D. (2006) Post-translational modifications regulating the activity and function of the nuclear factor kappa B pathway. *Oncogene* **25**, 6717–6730 https://doi.org/10.1038/sj.onc.1209937
24 Li, H., Wittwer, T., Weber, A., Schneider, H., Moreno, R., Maine, G.N. et al. (2012) Regulation of NF-κB activity by competition between relA acetylation and ubiquitination. *Oncogene* **31**, 611–623 https://doi.org/10.1038/onc.2011.253
25 Huang, B., Yang, X.D., Lamb, A. and Chen, L.F. (2010) Posttranslational modifications of NF-κB: another layer of regulation for NF-κB signalling pathway. *Cell. Signal.* **22**, 1282–1290 https://doi.org/10.1016/j.cellsig.2010.03.017
26 Lanucara, F., Lam, C., Mann, J., Monie, T.P., Colombo, S.A.P., Holman, S.W., et al. (2016) Dynamic phosphorylation of RelA on Ser42 and Ser45 in response to TNF a stimulation regulates DNA binding and transcription. *Open Biol.* **6**, 160055 https://doi.org/10.1098/rsob.160055
27 Chen, L.-F., Williams, S.A., Mu, Y., Nakano, H., Duerr, J.M., Buckbinder, L. et al. (2005) NF-κB RelA phosphorylation regulates RelA acetylation. *Mol. Cell. Biol.* **25**, 7966–7975 https://doi.org/10.1128/MCB.25.18.7966-7975.2005
28 Nihira, K., Ando, Y., Yamaguchi, T., Kagami, Y., Miki, Y. and Yoshida, K. (2010) Pim-1 controls NF-B signalling by stabilizing RelA/p65. *Cell Death Differ.* **17**, 689–698 https://doi.org/10.1038/cdd.2009.174
29 Campbell, K.J., Witty, J.M., Rocha, S. and Perkins, N.D. (2006) Cisplatin mimics ARF tumor suppressor regulation of RelA (p65) nuclear factor-κB transactivation. *Cancer Res.* **66**, 929–935 https://doi.org/10.1158/0008-5472.CAN-05-2234
30 Msaki, A., Sánchez, A.M., Koh, L.F., Barré, B., Rocha, S., Perkins, N.D. et al. (2011) The role of RelA (p65) threonine 505 phosphorylation in the regulation of cell growth, survival, and migration. *Mol. Biol. Cell* **22**, 3032–3040 https://doi.org/10.1091/mbc.e11-04-0280
31 Ferries, S., Perkins, S., Brownridge, P.J., Campbell, A., Eyers, P.A., Jones, A.R. et al. (2017) Evaluation of parameters for confident phosphorylation site localization using an orbitrap fusion tribrid mass spectrometer. *J. Proteome Res.* **16**, 3448–3459 https://doi.org/10.1021/acs.jproteome.7b00337
32 Chawade, A., Alexandersson, E. and Levander, F. (2014) Normalyzer: a tool for rapid evaluation of normalization methods for omics data sets. *J. Proteome Res.* **13**, 3114–3120 https://doi.org/10.1021/pr401264n
33 Huber, W., Von Heydebreck, A., Sültmann, H., Poustka, A. and Vingron, M. (2002) Variance stabilization applied to microarray data calibration and to the quantification of differential expression. *Bioinformatics* **18**, S96–S104 https://doi.org/10.1093/bioinformatics/18.suppl_1.S96
34 Mellacheruvu, D., Wright, Z., Couzens, A.L., Lambert, J.P., St-Denis, N.A., Li, T., et al. (2013) The CRAPome: a contaminant repository for affinity purification-mass spectrometry data. *Nat. Methods* **10**, 730–736 https://doi.org/10.1038/nmeth.2557
35 Szklarczyk, D., Gable, A.L., Lyon, D., Junge, A., Wyder, S., Huerta-Cepas, J., et al. (2019) STRING v11: protein-protein association networks with increased coverage, supporting functional discovery in genome-wide experimental datasets. *Nucleic Acids Res.* **47**, 607–613 https://doi.org/10.1093/nar/gky1131
36 Shannon, P., Markiel, A., Ozier, O., Baliga, N.S., Wang, J.T., Ramage, D. et al. 2003 Cytoscape: a software environment for integrated models of biomolecular interaction networks. *Genome Res.* **13**, 2498–2504 https://doi.org/10.1101/gr.1239303
37 Huang, D.W., Sherman, B.T. and Lempicki, R.A. (2009) Bioinformatics enrichment tools: paths toward the comprehensive functional analysis of large gene lists. *Nucleic Acids Res.* **37**, 1–13 https://doi.org/10.1093/nar/gkn923
38 Huang, D.W., Sherman, B.T. and Lempicki, R.A. (2009) Systematic and integrative analysis of large gene lists using DAVID bioinformatics resources. *Nat. Protoc.* **4**, 44–57 https://doi.org/10.1038/nprot.2008.211
39 Supek, F., Bošnjak, M., Škunca, N. and Šmuc, T. (2011) Revigo summarizes and visualizes long lists of gene ontology terms. *PLoS ONE* **6**, e21800 https://doi.org/10.1371/journal.pone.0021800
40 Kuznetsova, I., Lugmayr, A., Siira, S.J., Rackham, O. and Filipovska, A. (2019) CirGO: an alternative circular way of visualising gene ontology terms. BMC bioinformatics. *BMC Bioinformatics* **20**, 84 https://doi.org/10.1186/s12859-019-2671-2
41 Horn, H., Schoof, E.M., Kim, J., Robin, X., Miller, M.L., Diella, F. et al. (2014) Kinomexplorer: an integrated platform for kinome biology studies. *Nat. Methods* **11**, 603–604 https://doi.org/10.1038/nmeth.2968
42 Miller, M.L., Jensen, L.J., Diella, F., Jørgensen, C., Tinti, M., Li, L., et al. (2008) Linear motif atlas for phosphorylation-dependent signalling. *Sci. Signal.* **1**, ra2 https://doi.org/10.1126/scisignal.1159433
43 Colaert, N., Helsens, K., Martens, L., Vandekerckhove, J. and Gevaert, K. (2009) Improved visualization of protein consensus sequences by iceLogo. *Nat. Methods* **6**, 786–787 https://doi.org/10.1038/nmeth1109-786

44 Kuo, L.J. and Yang, L.X. (2008) γ-H2AX- A novel biomaker for DNA double-strand breaks. *In Vivo* **22**, 305–309 PMID:18610740
45 Ward, I.M. and Chen, J. (2001) Histone H2AX is phosphorylated in an ATR-dependent manner in response to replicational stress. *J. Biol. Chem.* **276**, 47759–47762 https://doi.org/10.1074/jbc.C100569200
46 Anderson, L.A. and Perkins, N.D. (2003) Regulation of relA (p65) function by the large subunit of replication factor C. *Mol. Cell. Biol.* **23**, 721–732 https://doi.org/10.1128/MCB.23.2.721-732.2003
47 Perkins, N.D., Felzien, L.K., Betts, J.C., Leung, K., Beach, D.H. and Nabel, G.J. (1997) Regulation of NF-κB by cyclin-dependent kinases associated with the p300 coactivator. *Science* **275**, 523–527 https://doi.org/10.1126/science.275.5299.523
48 Perkins, N.D., Agranoff, A.B., Pascal, E. and Nabel, G.J. (1994) An interaction between the DNA-binding domains of relA(p65) and Sp1 mediates human immunodeficiency virus gene activation. *Mol. Cell. Biol.* **14**, 6570–6583 https://doi.org/10.1128/MCB.14.10.6570
49 Girdwood, D., Bumpass, D., Vaughan, O.A., Thain, A., Anderson, L.A., Snowden, A.W. et al. (2003) P300 transcriptional repression is mediated by SUMO modification. *Mol. Cell* **11**, 1043–1054 https://doi.org/10.1016/S1097-2765(03)00141-2
50 Zhang, B., Wu, J., Cai, Y., Luo, M., Wang, B. and Gu, Y. (2018) AAED1 modulates proliferation and glycolysis in gastric cancer. *Oncol. Rep.* **40**, 1156–1164 https://doi.org/10.3892/or.2018.6478
51 Matsuoka, S., Ballif, B.A., Smogorzewska, A., McDonald, E.R., Hurov, K.E., Luo, J., et al. (2007) ATM and ATR substrate analysis reveals extensive protein networks responsive to DNA damage. *Science* **316**, 1160–1166 https://doi.org/10.1126/science.1140321
52 Boeing, S., Williamson, L., Encheva, V., Gori, I., Saunders, R.E., Instrell, R., et al. (2016) Multiomic analysis of the UV-induced DNA damage response. *Cell Rep.* **15**, 1597–1610 https://doi.org/10.1016/j.celrep.2016.04.047
53 Nicolai, S., Mahen, R., Raschellà, G., Marini, A., Pieraccioli, M., Malewicz, M. et al. (2020) ZNF281 is recruited on DNA breaks to facilitate DNA repair by non-homologous end joining. *Oncogene* **39**, 754–766 https://doi.org/10.1038/s41388-019-1028-7
54 Enserink, J.M. and Kolodner, R.D. (2010) An overview of Cdk1-controlled targets and processes. *Cell Div.* **5**, 1–41 https://doi.org/10.1186/1747-1028-5-11
55 Gonzalez, F.A., Raden, D.L. and Davis, R.J. (1991) Identification of substrate recognition determinants for human ERK1 and ERK2 protein kinases. *J. Biol. Chem.* **266**, 22159–22163 https://doi.org/10.1016/S0021-9258(18)54548-8
56 Fang, L., Choudhary, S., Zhao, Y., Edeh, C.B., Yang, C., Boldogh, I. et al. (2014) ATM regulates NF-κB-dependent immediate-early genes via RelA ser 276 phosphorylation coupled to CDK9 promoter recruitment. *Nucleic Acids Res.* **42**, 8416–8432 https://doi.org/10.1093/nar/gku529
57 Traven, A. and Heierhorst, J. (2005) SQ/TQ cluster domains: concentrated ATM/ATR kinase phosphorylation site regions in DNA-damage-response proteins. *BioEssays* **27**, 397–407 https://doi.org/10.1002/bies.20204
58 Roskoski, R. (2012) ERK1/2 MAP kinases: structure, function, and regulation. *Pharmacol. Res.* **66**, 105–143 https://doi.org/10.1016/j.phrs.2012.04.005
59 Cargnello, M. and Roux, P.P. (2011) Activation and function of the MAPKs and their substrates, the MAPK-activated protein kinases. *Microbiol. Mol. Biol. Rev.* **75**, 50–83 https://doi.org/10.1128/MMBR.00031-10
60 Wang, Y., Xu, J., Gao, G., Li, J., Huang, H., Jin, H. et al. (2016) Tumor-suppressor NFκB2 p100 interacts with ERK2 and stabilizes PTEN mRNA via inhibition of MIR-494. *Oncogene* **35**, 4080–4090 https://doi.org/10.1038/onc.2015.470
61 Gatei, M., Young, D., Cerosaletti, K.M., Desai-Mehta, A., Spring, K., Kozlov, S. et al. (2000) ATM-dependent phosphorylation of nibrin in response to radiation exposure. *Nat. Genet.* **25**, 115–119 https://doi.org/10.1038/75508
62 Wu, X., Ranganathan, V., Weisman, D.S., Heine, W.F., Ciccone, D.N., Neill, T.B.O., et al. (2000) ATM phosphorylation of Nijmegen breakage syndrome protein is required in a DNA damage response. *Nature* **405**, 477–482 https://doi.org/10.1038/35013089
63 Tando, T., Ishizaka, A., Watanabe, H., Ito, T., Iida, S., Haraguchi, T., et al. (2010) Requiem protein links RelB/p52 and the Brm-type SWI/SNF complex in a noncanonical NF-κB pathway. *J. Biol. Chem.* **285**, 21951–21960 https://doi.org/10.1074/jbc.M109.087783
64 Mulero, M.C., Shahabi, S., Ko, M.S., Schiffer, J.M., Huang, D.B., Wang, V.Y.F. et al. (2018) Protein cofactors are essential for high-Affinity DNA binding by the nuclear factor κb relA subunit. *Biochemistry* **57**, 2943–2957 https://doi.org/10.1021/acs.biochem.8b00158
65 Hegde, V., Yadavilli, S. and Deutsch, W.A. (2007) Knockdown of ribosomal protein S3 protects human cells from genotoxic stress. *DNA Repair (Amst)* **6**, 94–99 https://doi.org/10.1016/j.dnarep.2006.09.004
66 Pennington, K., Chan, T., Torres, M. and Andersen, J. (2018) The dynamic and stress-adaptive signalling hub of 14-3-3: emerging mechanisms of regulation and context-dependent protein–protein interactions. *Oncogene* **37**, 5587–5604 https://doi.org/10.1038/s41388-018-0348-3
67 Zuo, S., Xue, Y., Tang, S., Yao, J., Du, R., Yang, P. et al. (2010) 14-3-3 epsilon dynamically interacts with key components of mitogen-activated protein kinase signal module for selective modulation of the TNF-aα-Induced time course-dependent NF-κb activity. *J. Proteome Res.* **9**, 3465–3478 https://doi.org/10.1021/pr9011377
68 Milton, A.H., Khaire, N., Ingram, L., O'Donnell, A.J. and La Thangue, N.B. (2006) 14-3-3 proteins integrate E2F activity with the DNA damage response. *EMBO J.* **25**, 1046–1057 https://doi.org/10.1038/sj.emboj.7600999